ROYAL SOCIETY
OF CHEMISTRY

In situ Study of Au Nanoparticle Formation in a Mechanochemical-Aging-Based Method

Austin J. Richard, Michael Ferguson, Blaine G. Fiss, Hatem M. Titi, Jesus Valdez, Nikolas Provatas, Tomislav Friščić, and Audrey Moores

Supplemental Information

1) Analytical Methods

X-ray photoelectron spectroscopy (XPS)

XPS was used to track the chemical transformation of Au(III) precursor to Au (I) and Au(0) products in the solid state. Milled powders were evenly spread over single-sided adhesive Cu tape and mounted onto the sample block. Powders aged at elevated or lowered temperatures quickly equilibrated to room temperature on the sample block, assuring a consistent scanning temperature. Samples were analyzed on a Fischer Scientific Kα X-Ray spectrometer with an excitation source of Al Kα = 1486.6 eV. The spot size was 400 μm, running three survey scans at 200 mV with 50 ms residence times, five high-resolution scans for C, and 10 high-resolution scans for other specific elements, also at residence times of 50 ms. Au scans were always the first to be performed as Au(III) is known to photoreduce during XPS analysis, likely caused by the low energy electrons emitted by the flood gun for charge balancing. Data was processed using the Avantage software. A Shirley-type background subtraction was performed before the binding energies were charge corrected by referencing to the C 1s binding energy at 284.8 eV. Peak position and deconvolution were also performed. For peak fitting, pure Gaussian distributions were employed with initial separation of 3.7 eV and peaks were then fitted by a least squares algorithm without any constraints. Deconvoluted peak profiles were integrated and subsequently plotted using a custom-built Python3 script to reveal the percentage reduction of the gold salt. Au(III), Au(I) and Au(0) were considered during deconvolution.

Diffuse reflectance spectroscopy (DRS)

Milled powders were placed into clean and dry 10 mm wide quartz cuvettes for DRS analysis. Samples were analysed using a Perkin Elmer Lambda 750 UV/Vis/NIR spectrophotometer equipped with tungsten-halogen and deuterium light sources, a double holographic grating monochromator, a high sensitivity R928 photomultiplier for UV/Vis and a Peltier cooled PbS detector for NIR. Diffuse reflectance measurements from 850 to 350 nm, in 1 nm increments at a scan speed of 266.75 nm/min, were done through the Scan Lambda 750 software program. $BaSO_4$ white powder was used in place of a Spectralon standard as a highly reflective solid upon which a 100% reflection (0 Absorbance) correction was performed. The instrument then measured the percent diffuse reflectance of the sample relative to the standard and calculated an absorbance value through a logarithmic transformation of the percent reflectance. DRS data was exported through the UV WinLab software and then normalized and plotted using Python3. In all cases triplicate 'b' is presented in the main text.

Powder X-ray diffraction (PXRD)

PXRD studies were performed using a Bruker D8 Advance diffractometer equipped with a Ni-filtered CuKα (λ = 1.5418 Å) source, 1D LYNXEYE detector, and operating at 40kV and 40 mA. Individual PXRD patterns were obtained over a 2ϑ range of 3° to 90° in increments of 0.02° with an exposure time of 0.75 s. The neat powders were spread evenly over a silicon wafer of a low-zero background sample holder. In all cases triplicate 'b' is presented in the main text.

In situ aging studies were performed by fitting an Anton Paar CHC⁺ chamber to the diffractometer, where the sample area was filled, and levelled, with freshly milled powder. For constant temperature studies diffractograms were collected over a 2ϑ range of 5° to 50° in increments of 0.02° with an exposure time of 0.8 s in a stepwise fashion. In total 120 diffractograms were obtained for each temperature (30, 35, and 40 °C).

For the variable temperature study diffractograms were collected 2ϑ range of 32.5° to 42.5° in increments of 0.02° with an exposure time of 2.8 s in a stepwise fashion. The initial temperature was set equal to 24 °C and was increased by 2 °C after every five consecutive measurements. The study was complete after the fifth measurement at 46 °C.

Transmission electron microscopy (TEM)

The TEM and scanning transmission electron microscopy (STEM) studies were performed using a Thermo Scientific Talos F200X transmission electron microscope equipped with a high-brightness XFEG Schottky source, operated at 200 keV.

TEM grids were prepared using the drop-cast method whereby a 7.5 µL of a 1.0 mg mL^{-1} solution of the milled powder in toluene was drop-cast onto a 400 mesh Cu grid allowed to dry. Images were captured in the bright field mode. Individual particles were sized using the ImageJ software in populations of N ≥ 600 and the resulting size distribution analysis was performed using Microsoft Excel. The resulting population profiles from the number distributions were fitted to Gaussian functions in the Fityk program[54] and plotted using Python3. Uncertainties in the form of standard deviations were pulled from the fitted Gaussian functions made by Fityk.

STEM sample grids were prepared in the solid-state. A 200 mesh Cu grid with a 15 nm thick SiOx substrate coating was impregnated with the milled powder by introducing the grid into the sample and agitating the recipient. Once impregnated, pressurized air was used to remove excess sample from the grid. The sample was analyzed using STEM coupled with the high-angle annular dark field (HAADF) detector.

The energy dispersive X-ray spectroscopy (EDXS) analyses were performed using a SDD Super-X detector at 200 keV. The total acquisition time was 15 min per sample using drift correction to compensate the shift after each scan.

2) **Results and discussion**

a. **Visual Inspection**

The colors of the powders shown in Figure S1 exhibit some variation to those observed in real life, caused by differences in lighting and by the automatic brightness and contrast adjustments performed by the camera. This is particularly true for samples aged at 32 °C where the samples darkened consistently after seven days of aging to appear dark purple/black after 43 days.
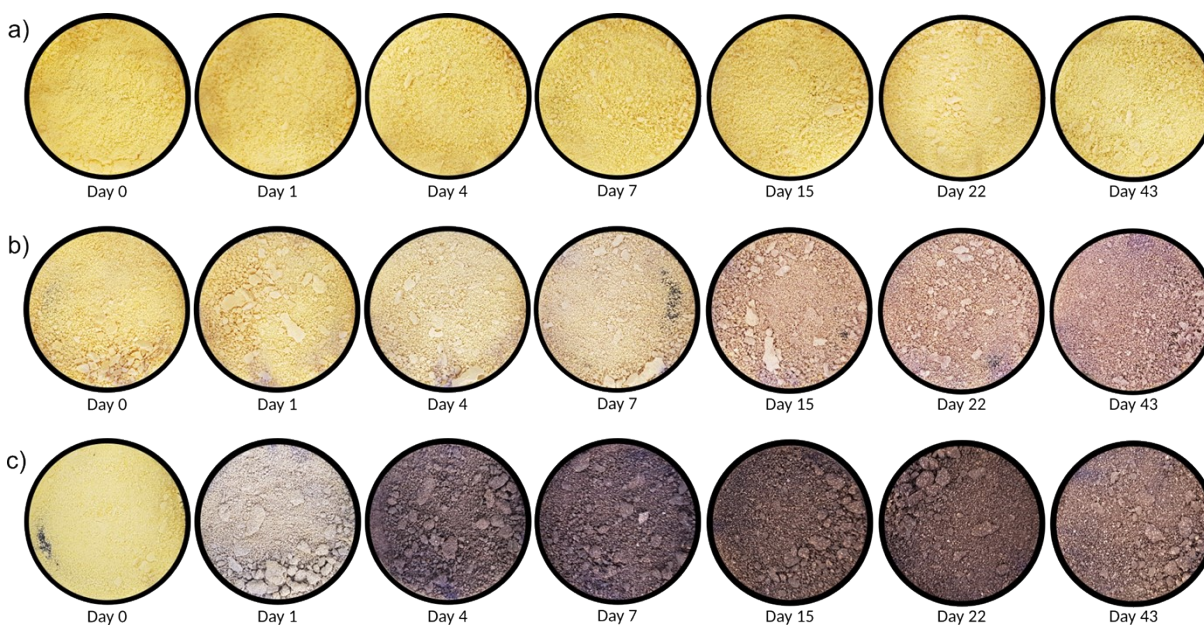

a)

| Day 0 | Day 1 | Day 4 | Day 7 | Day 15 | Day 22 | Day 43 |

b)

| Day 0 | Day 1 | Day 4 | Day 7 | Day 15 | Day 22 | Day 43 |

c)

| Day 0 | Day 1 | Day 4 | Day 7 | Day 15 | Day 22 | Day 43 |

Figure S1 Macroscopic photos showing the changing color of the milled powders over the aging period. Powders were aged at a) -18 °C, b) 21 °C, and c) 32 °C.

b. **Reducing agent selection**

This color change and XPS were used to screen reducing agents. $NaBH_4$ and ascorbic acid reacted too quickly to allow for the desired monitoring. More specifically, the colour of the powder was already deep red upon opening the grinding jar and XPS of the freshly milled sample showed almost quantitative reduction from Au(III) to Au(0). In the case of hydroquinone, we did not observe any colour change in the material upon grinding. However, the data obtained from XPS analysis consistently exhibited a signal-to-noise ratio that would be unsuitable for peak fitting and subsequent deconvolution.

c. **X-ray photoelectron spectroscopy**

Investigating the photoreduction of HAuCl$_4\cdot$3H$_2$O

The propensity of Au(III) salts to undergo photoreduction during XPS analysis increases the difficulty in tracking the reaction using the technique. To better understand the process analyses were performed on HAuCl$_4\cdot$3H$_2$O as received from the supplier. Granules of the solid reactant were pressed onto the adhesive Cu tape with a flat PTFE coated spatula, to avoid galvanic reduction. Two spots of the sample were selected for analysis. On the first, five scans of Au were performed, (Figure S2a), which was then repeated to give a total of ten scans, (Figure S2b). On the second, ten scans of Au were performed in a single step, (Figure S2c). The reduction of Au(III) to Au(0) is clear in each of the three analyses. After five scans (a), the gold salts has been reduced by 14 %, given by the area of the purple and blue peaks which represent the Au(0) doublet. After the second five scans (b) the gold salt was further reduced, for a total of 20 %. When ten scans were performed sequentially (c) the same amount of reduction was observed, 20 %. Given the high levels of reduction observed after just five scans, 14 %, which is increased by just 6 % after the further five scans, we believe that the reduction depends on the amount of time the sample is being measured rather than the number of scans. Given that the ten-scan run gives the same amount of reduction, we suspect that the low energy electron emitting flood gun, used for charge correction in the sample, is responsible for the observed reduction.
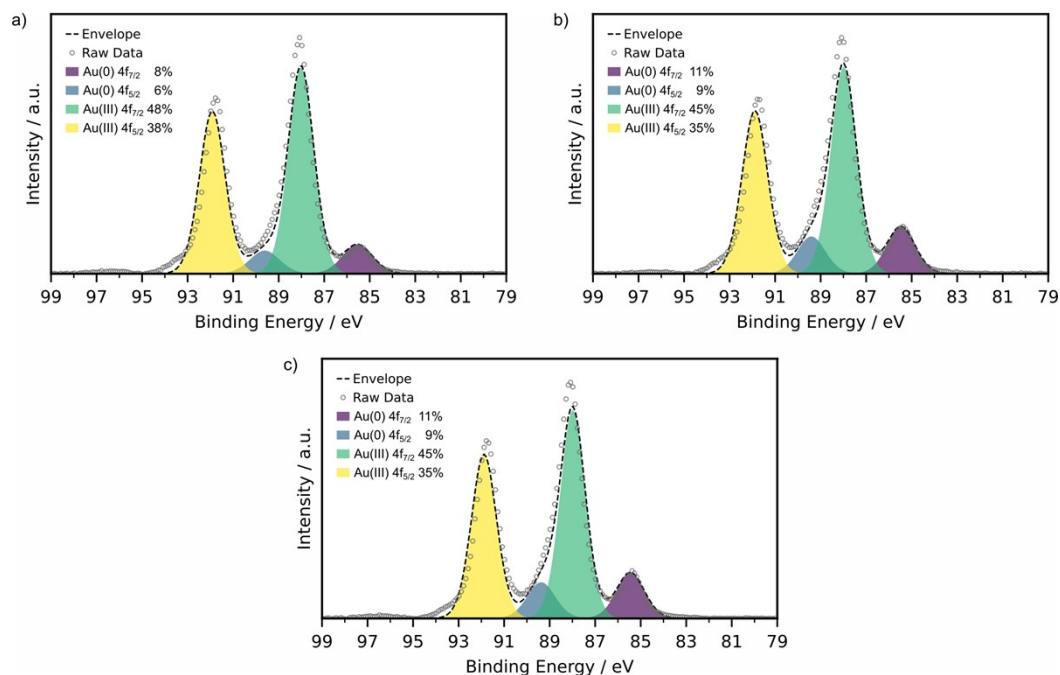
Figure S2 Normalized deconvolutions of the XPS spectra for $HAuCl_4 \cdot 3H_2O$ after a) five scans, b) a further five scans of the same spot, and c) ten scans of another region. Purple and blue peaks represent the Au(0) $4f_{7/2}$ and $4f_{5/2}$ signals, respectively, while green and yellow peaks represent the Au(III) $4f_{7/2}$ and $4f_{5/2}$ signals, respectively.

Attempts were made to perform the analyses with the flood gun turned off in an effort to avoid the photoreduction of the gold salt. Three spots were analyzed for a sample of freshly milled powder, Figure S3. If it evident that turning off the flood gun had adverse effects on the obtained data. Peaks were shifted considerably and inconsistently which also resulted in a great deal of peak broadening. The combination of these effected rendered the charge correction and deconvolution of the raw peaks into the Au(0) and Au(III) doublets impossible.
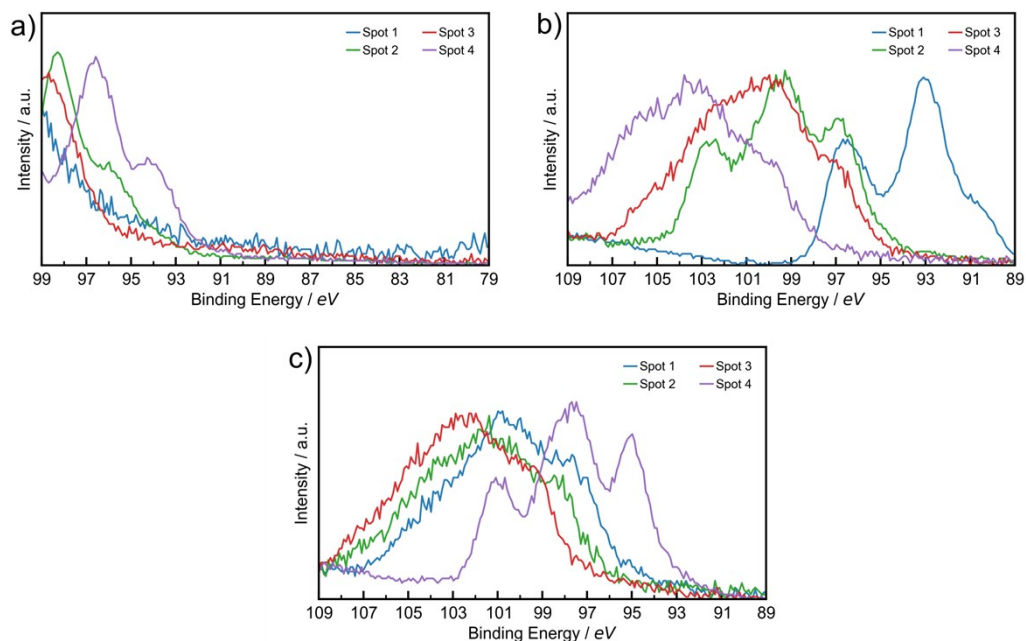
Figure S3 XPS results of a standard day 0 milled powder with the low energy electron emitting flood gun turned off. Plots a), b), and c) represent three individual samples of the milled powder.

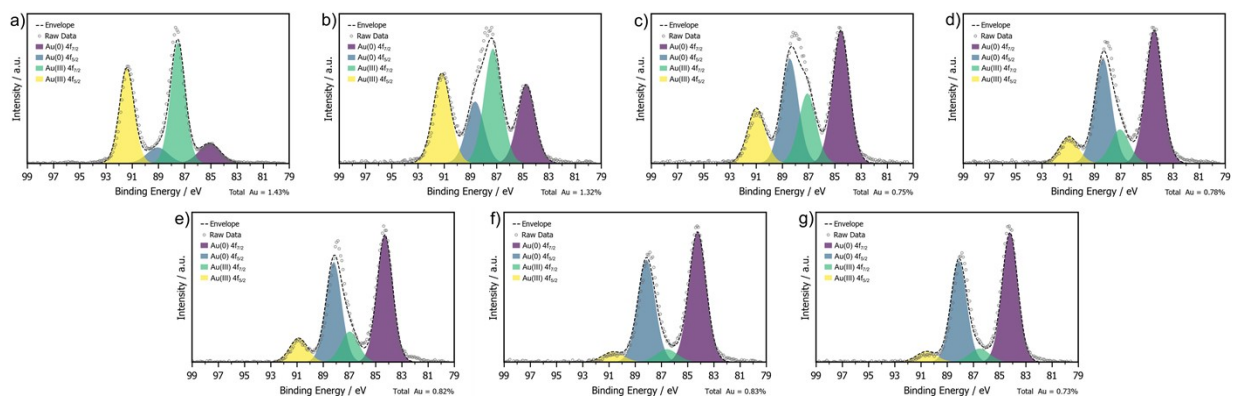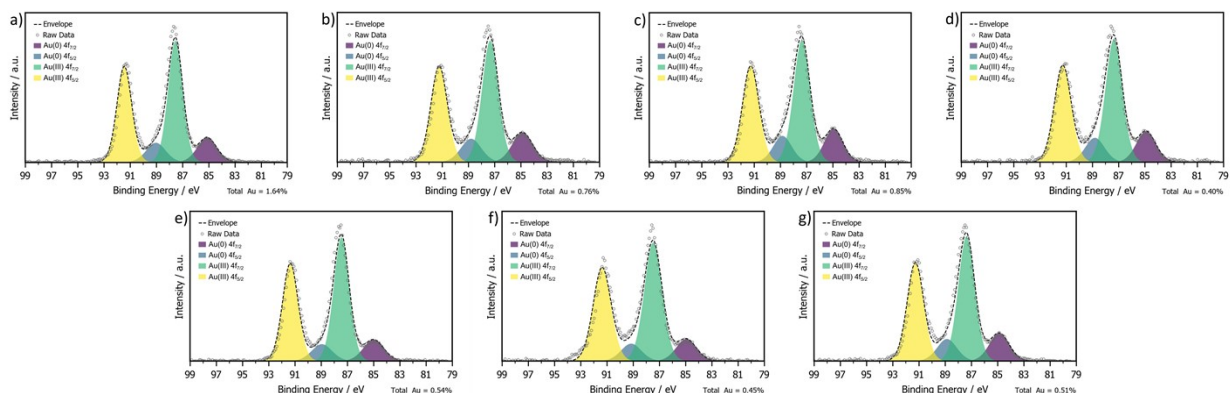## XPS monitoring of samples during the six-week aging period

Figure S4 Normalized deconvolutions of the XPS data for milled powder aged at 21 °C. The purple and blue peaks represent the Au(0) $4f_{7/2}$ and $4f_{5/2}$ signals, respectively. The green and yellow peaks represent the Au(III) $4f_{7/2}$ and $4f_{5/2}$ signals, respectively. Plots correspond to aging times of a) 0 days, b) 1 day, c) 4 days, d) 7 days, e) 15 days, f) 22 days, and g) 43 days.
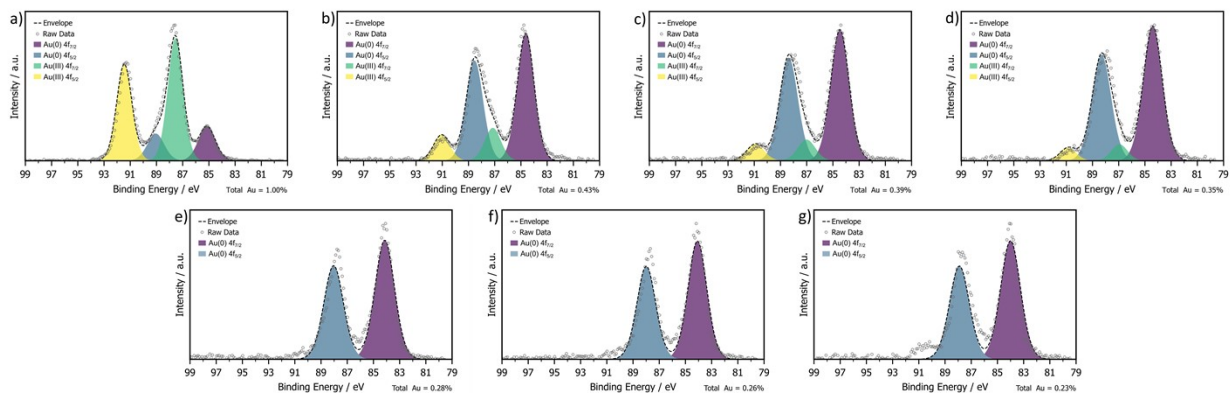
Figure S5 Normalized deconvolutions of the XPS data for milled powder aged at -18 °C. The purple and blue peaks represent the Au(0) $4f_{7/2}$ and $4f_{5/2}$ signals, respectively. The green and yellow peaks represent the Au(III) $4f_{7/2}$ and $4f_{5/2}$ signals, respectively. Plots correspond to aging times of a) 0 days, b) 1 day, c) 4 days, d) 7 days, e) 15 days, f) 22 days, and g) 43 days.

Figure S6 Normalized deconvolutions of the XPS data for milled powder aged at 32 °C. In plots a-d, the purple and blue peaks represent the Au(0) $4f_{7/2}$ and $4f_{5/2}$ signals and the green and yellow peaks represent the Au(III) $4f_{7/2}$ and $4f_{5/2}$ signals, respectively. In plots e-g, the best fitting was found without any Au(III) peak. Plots correspond to aging times of a) 0 days, b) 1 day, c) 4 days, d) 7 days, e) 15 days, f) 22 days, and g) 43 days.

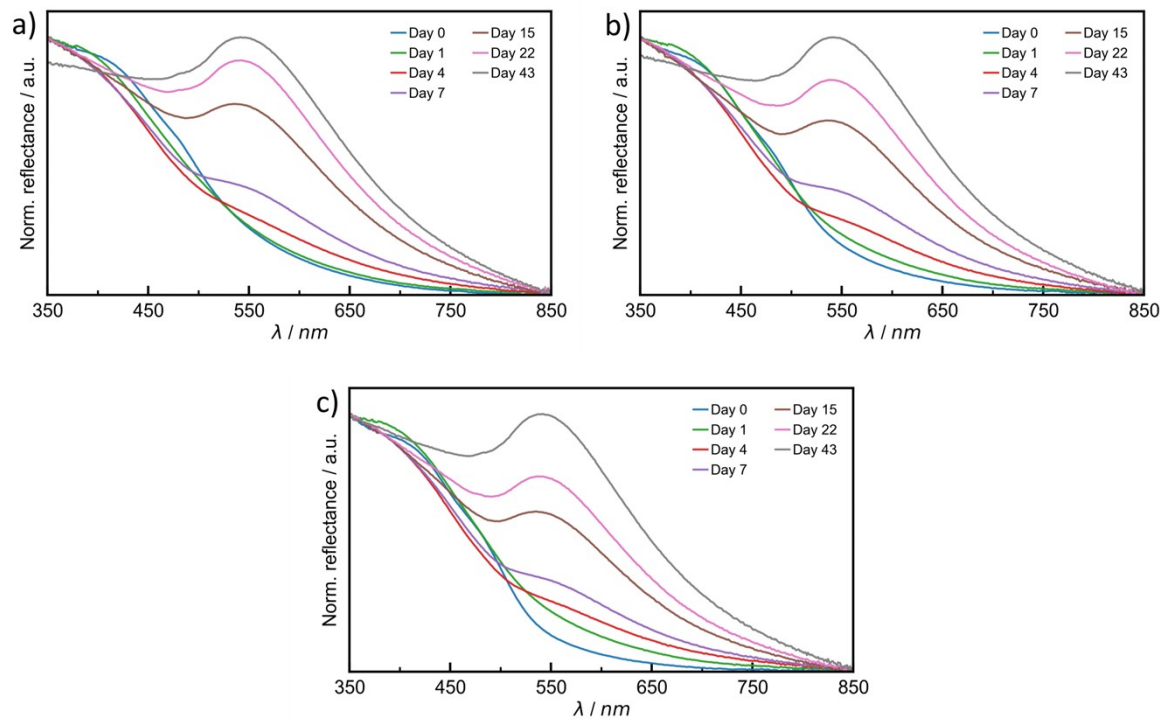### d. Diffuse reflectance spectroscopy

Figure S7 DRS plots for triplicates a, b, and c aged at 21 °C. Samples were analyzed after 0 (blue), 1 (green), 4 (red), 7 (violet), 15 (brown), 22 (pink), and 43 (grey) days of aging.
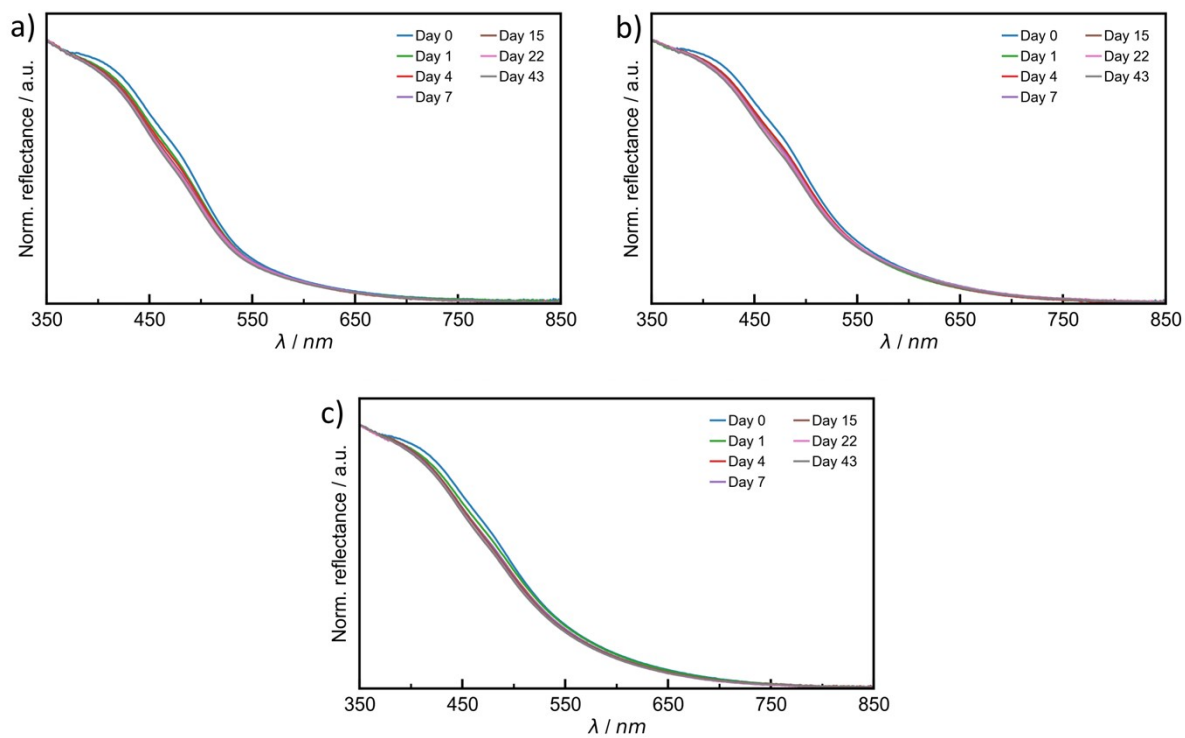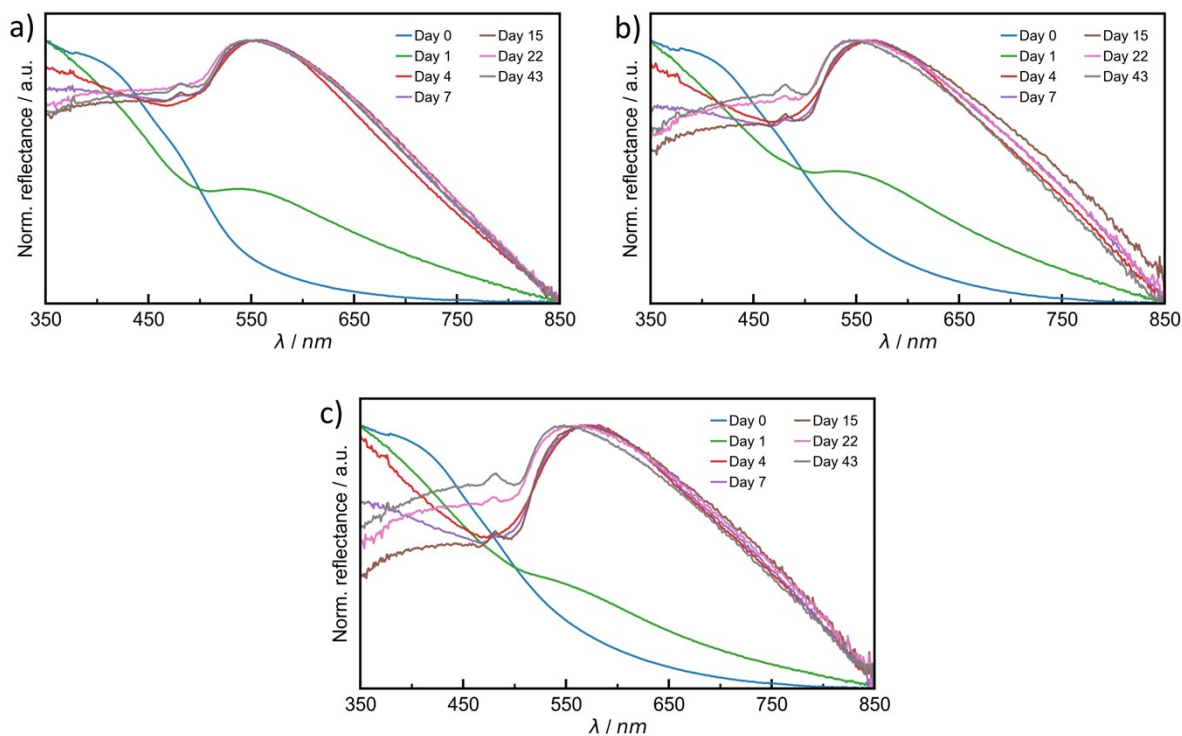
Figure S8 DRS plots for triplicates a, b, and c aged at -18 °C. Samples were analyzed after 0 (blue), 1 (green), 4 (red), 7 (violet), 15 (brown), 22 (pink), and 43 (grey) days of aging.

Figure S9 DRS plots for triplicates a, b, and c aged at 32 °C. Samples were analyzed after 0 (blue), 1 (green), 4 (red), 7 (violet), 15 (brown), 22 (pink), and 43 (grey) days of aging.

The absorption activity between the wavelengths of 750 nm to 350 nm is overwhelmingly due to the Au(III) and Au(0) species and does not originate from other materials, precursor or by-product, in the solid (Figure S10).
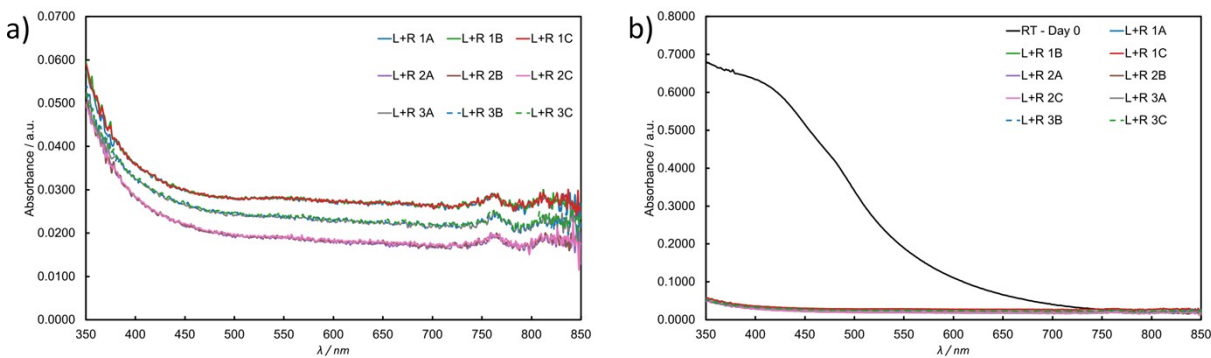

Figure S10 a) DRS raw data plot of a 5:1.1 molar mixture of octadecylamine (L = ligand) and trisodium citrate dihydrate (R = reductant). b) The same plot nominally compared to a standard day 0 absorbance curve of the milled powder with the gold-salt.
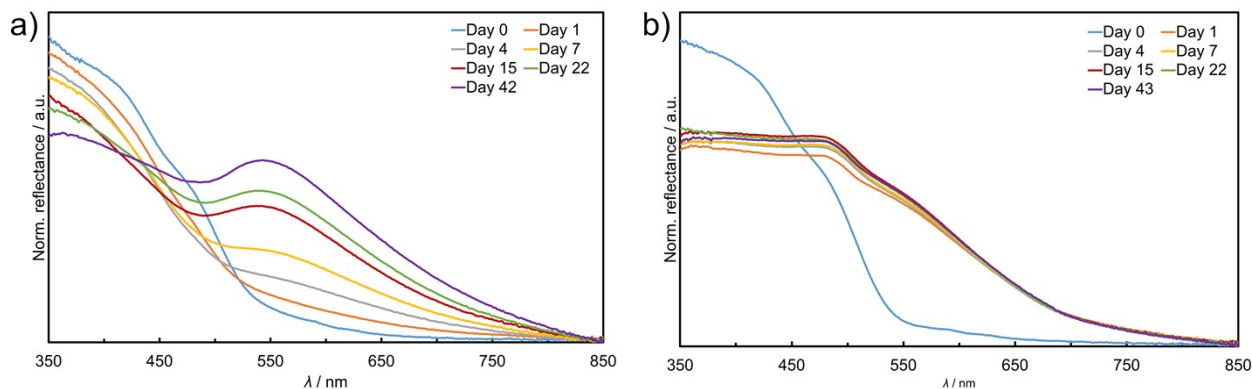
Figure S11 a) NaCt blank. A DRS plot of a 5:1 molar mixture of octadecylamine and tetrachloroauric acid (III) trihydrate aged at 21 °C for 42 days. b) ODA blank. A DRS plot of a 5:1 molar mixture of trisodium citrate dihydrate and tetrachloroauric acid (III) trihydrate aged at 21 °C for 42 days.

The DRS study showed gradual increase in absorbance observed for samples aged at 21 °C. Plotting the normalized absorbance values at 541 nm, the position of maximum absorbance reveals a sigmoidal relationship. As the data does not begin at exactly zero, a logistic function (Equation S1) was fitted to the data using Python3.

$$S(x) = \frac{L}{1 + exp^{-k(x - x_{0)}}} + b \qquad \textbf{Equation S1}$$

Where L scales the function to the range of the input absorbance data, k indicates the steepness of the curve, x_0 is the midpoint of the sigmoid in x, and b accounts for the offset in the absorbance data which is not initially 0 for freshly milled powder.

The resulting logistic function was found to be,

$$S(x) = \frac{0.917}{1 + exp^{-0.146(x - 11.414)}} + 0.088 \qquad \textbf{Equation S2}$$

With an r^2 value of 0.999 for the fitting.

Data points between 0 and 22 days of aging showed a linear trend, these were fitting to a straight line in Python3. The gradient of the resulting straight line gave a rate of growth of $k = 3.43 x 10^{-7}$ s^{-1}. In this case, $r^2 = 0.982$.
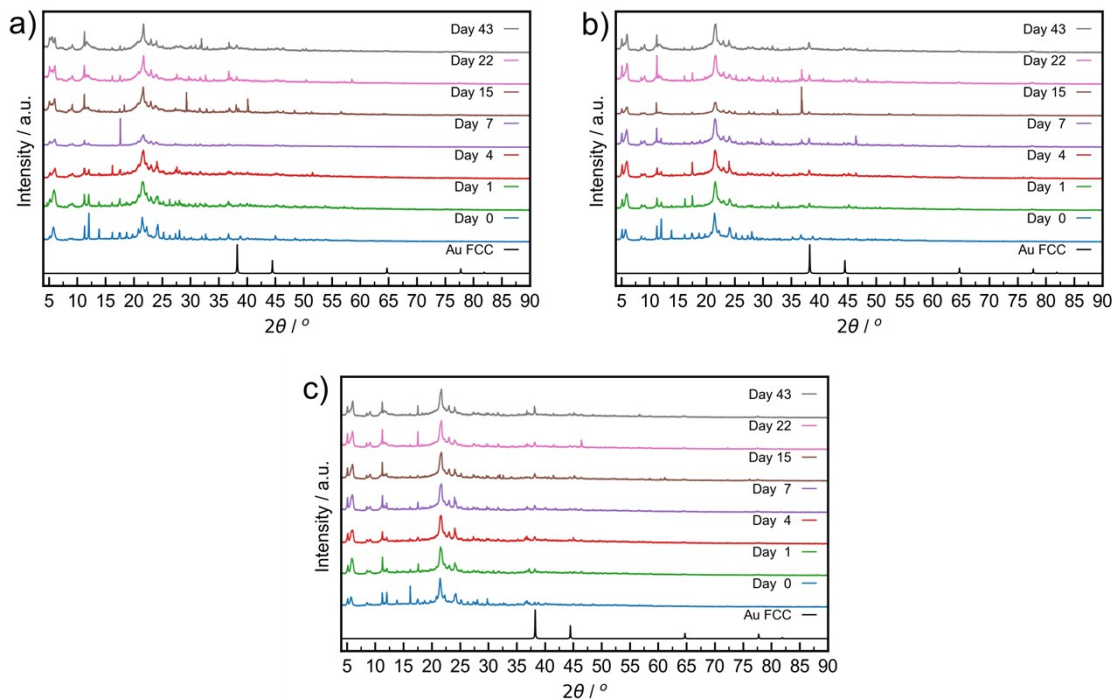
e. Powder X-ray diffraction

Figure S12 PXRD plots for triplicates a, b, and c at 21 °C. Samples were analyzed after 0 (blue), 1 (green), 4 (red), 7 (violet), 15 (brown), 22 (pink), and 43 (grey) days of aging. The simulated pattern for elemental gold in the FCC lattice[55] is plotted in black.
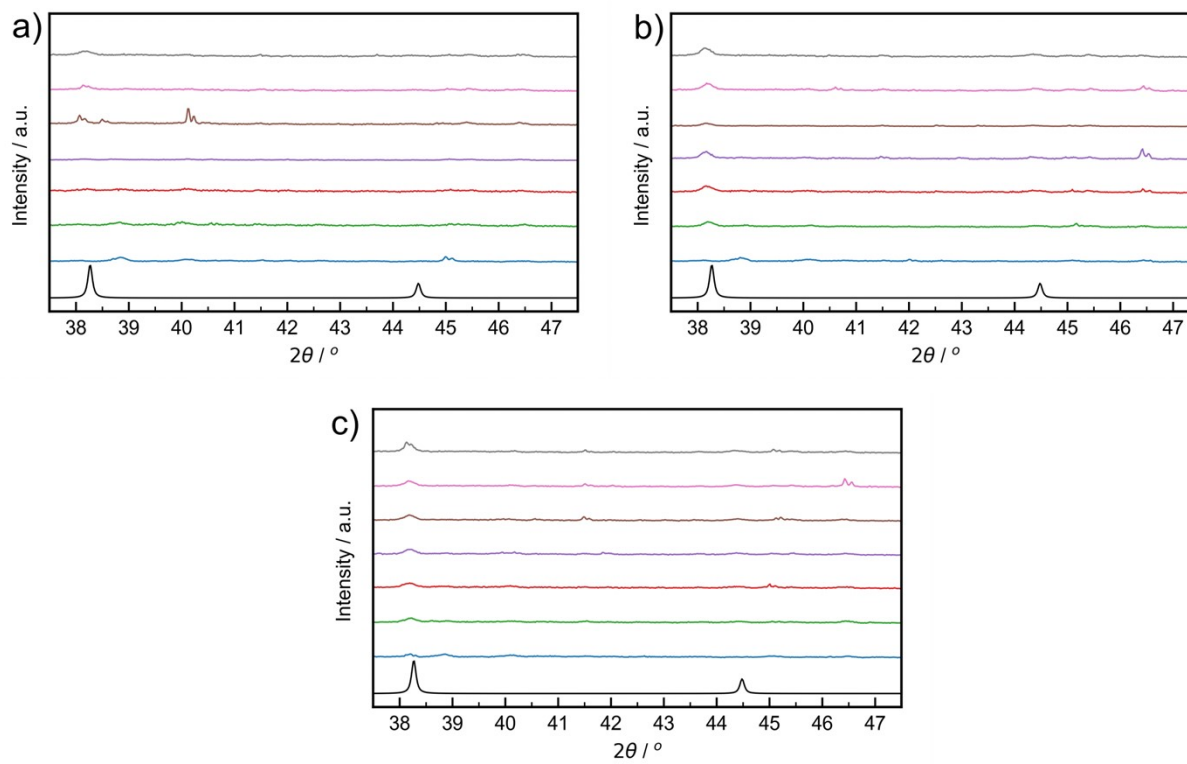
Figure S13 Zoomed PXRD plots between 37.5° and 47.5° for triplicates a, b, and c at 21 °C. Samples were analyzed after 0 (blue), 1 (green), 4 (red), 7 (violet), 15 (brown), 22 (pink), and 43 (grey) days of aging. The simulated pattern for elemental gold in the FCC lattice[55] is plotted in black.
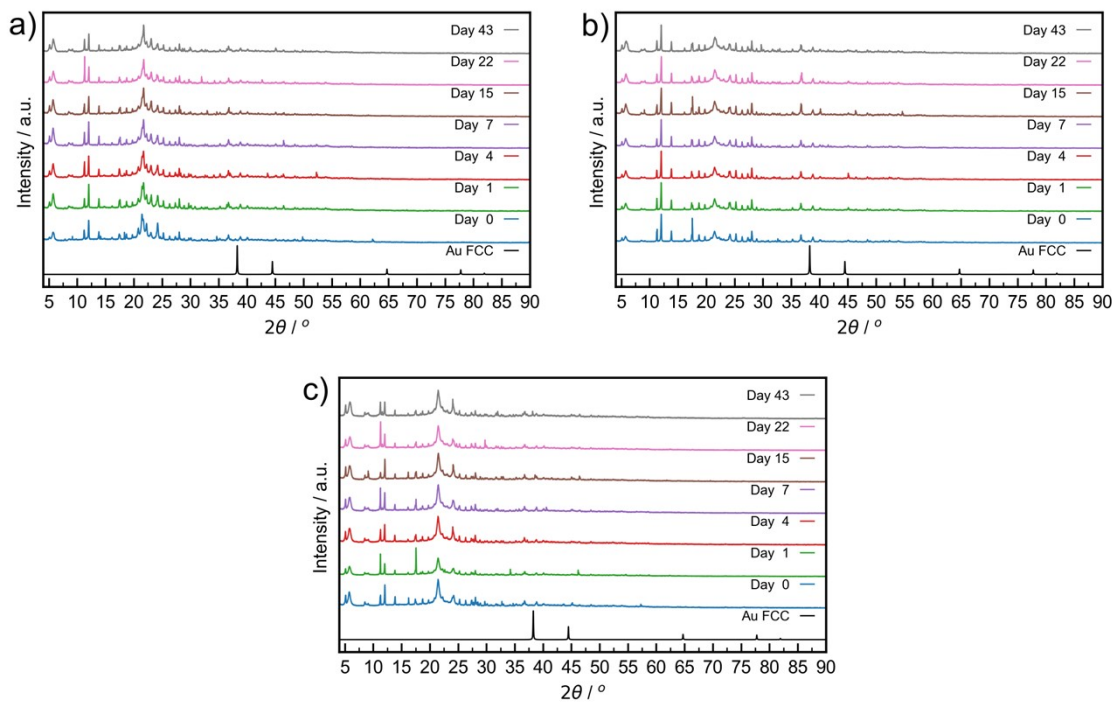
Figure S14 PXRD plots for triplicates a, b, and c aged at -18 °C. Samples were analyzed after 0 (blue), 1 (green), 4 (red), 7 (violet), 15 (brown), 22 (pink), and 43 (grey) days of aging. The simulated pattern for elemental gold in the FCC lattice[55] is plotted in black.
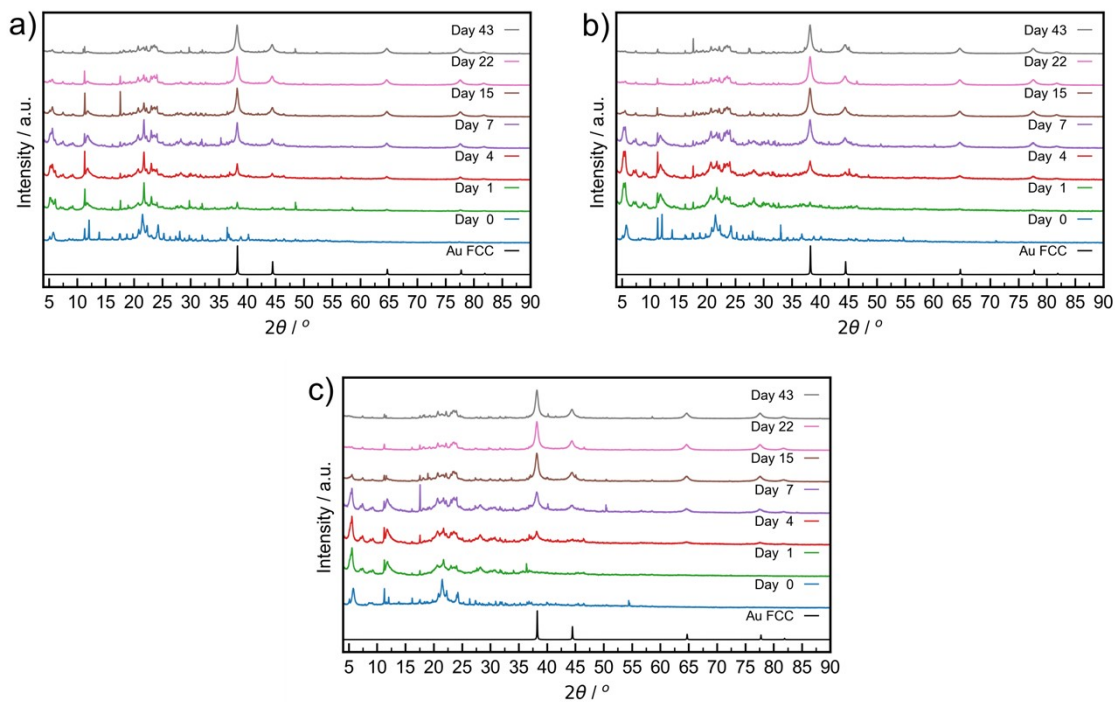
Figure S15 PXRD plots for triplicates a, b, and c aged at 32 °C. Samples were analyzed after 0 (blue), 1 (green), 4 (red), 7 (violet), 15 (brown), 22 (pink), and 43 (grey) days of aging. The simulated pattern for elemental gold in the FCC lattice[55] is plotted in black.
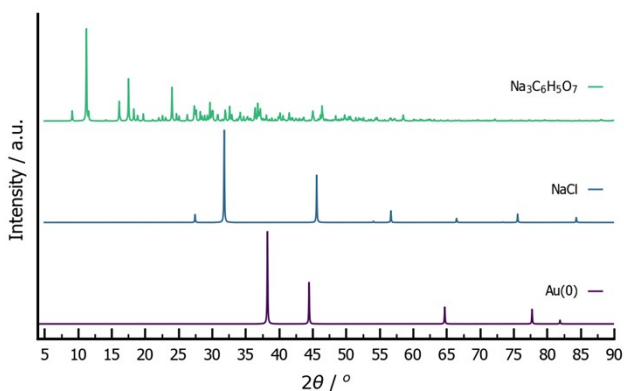

Figure S16 Simulated PXRD patterns of elemental gold in the FCC lattice (purple),[55] NaCl (blue),[56] and trisodium citrate dihydrate (green).[57]

f. Transmission electron microscopy

Discussion S1: Blank test for drop cast TEM sample preparation: We tested the effect of the drop casting method on samples prior to any mechanical activation or aging. The three reactants (HAuCl$_4$, NaCt, ODA) were stirred in toluene for 120 s in a solid-to-liquid ratio of 1 mg mL^{-1}. All these reagents are insoluble in toluene. Analysis of a sample taken from this solution revealed the presence of NPs with an average particle diameter (Ø) of 4.1 ± 1.7 nm (Figure S18). These particles observed by scanning transmission electron microscopy coupled with a high-angle annular dark field detector (STEM-HAADF) were confirmed to be AuNPs by energy dispersive X-ray spectroscopy (EDXS). Signals corresponding to Au are correlated to the particles observed in the STEM-HAADF image, whereas the Cl signal is evenly dispersed throughout the imaged area (Figure S19). This sample shows that suspension in toluene is in itself sufficient to cause the formation of Au(0) NPs, of sizes around 4 nm.
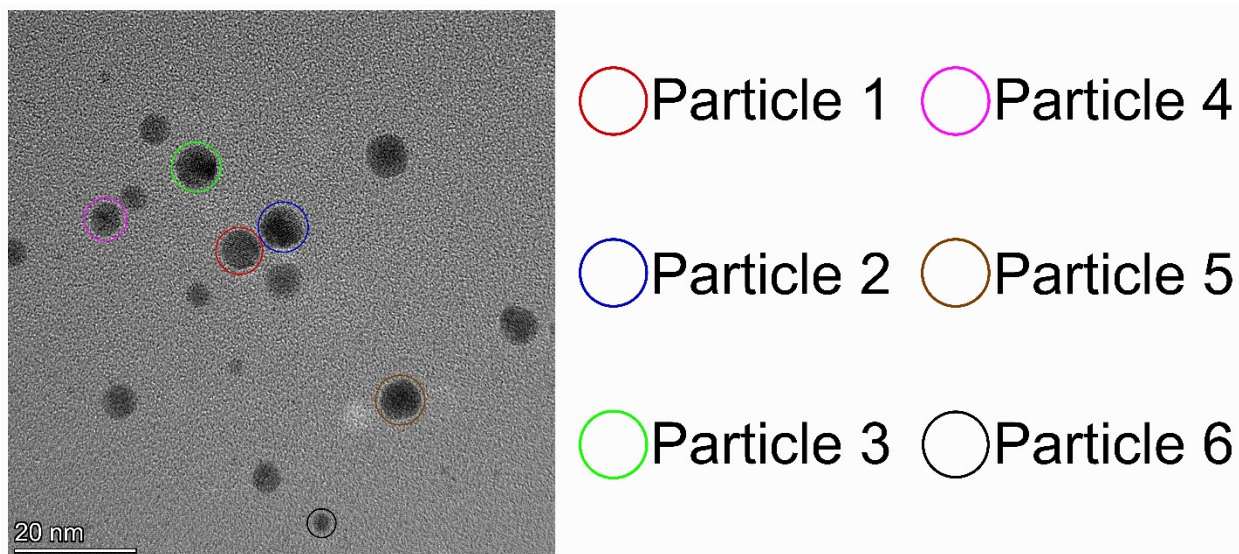

Figure S17 High resolution TEM micrograph of AuNPs with a spherical morphology. Particles with good diffraction have been picked out, circled, and have had their lattice fringes measured. All particle were found to be in good agreement with the (111) d-spacing of FCC Au(0).
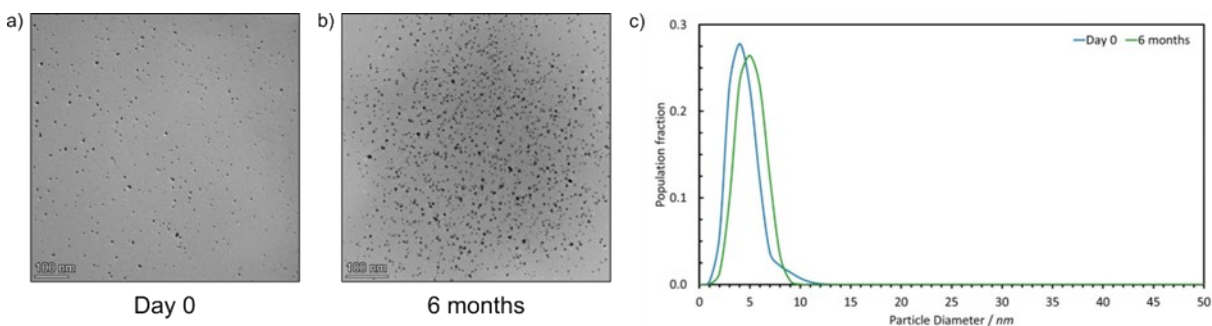
Day 0   6 months

Figure S18 TEM drop-cast images (a, b) and population sizing (c) of nanoparticles produced via a solution control test. Tetrachloroauric acid trihydrate, octadecylamine, and trisodium citrate dihydrate (1:5:1.1 molar ratios) were added to 100 mL of toluene at a solid-to-liquid ratio of 1 mg mL^{-1} and stirred at 400 rpm for 2 minutes at room temperature (21 °C), simulating the drop-casting process. On day 0 (blue), nanoparticles averaged 4.05 ± 1.66 nm in diameter. After 6 months of sitting on the TEM grid after dropcasting (green), nanoparticles averaged 4.71 ± 1.34 nm.
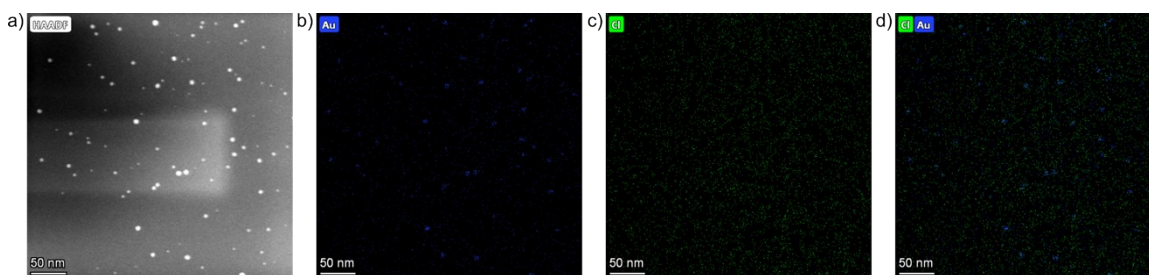

Figure S19 STEM-HAADF images and EDXS elemental maps for Au, Cl, and Au combined with Cl (left to right, respectively) for the solution control sample where the three reactants were stirred in toluene for 120 s before drop casting.
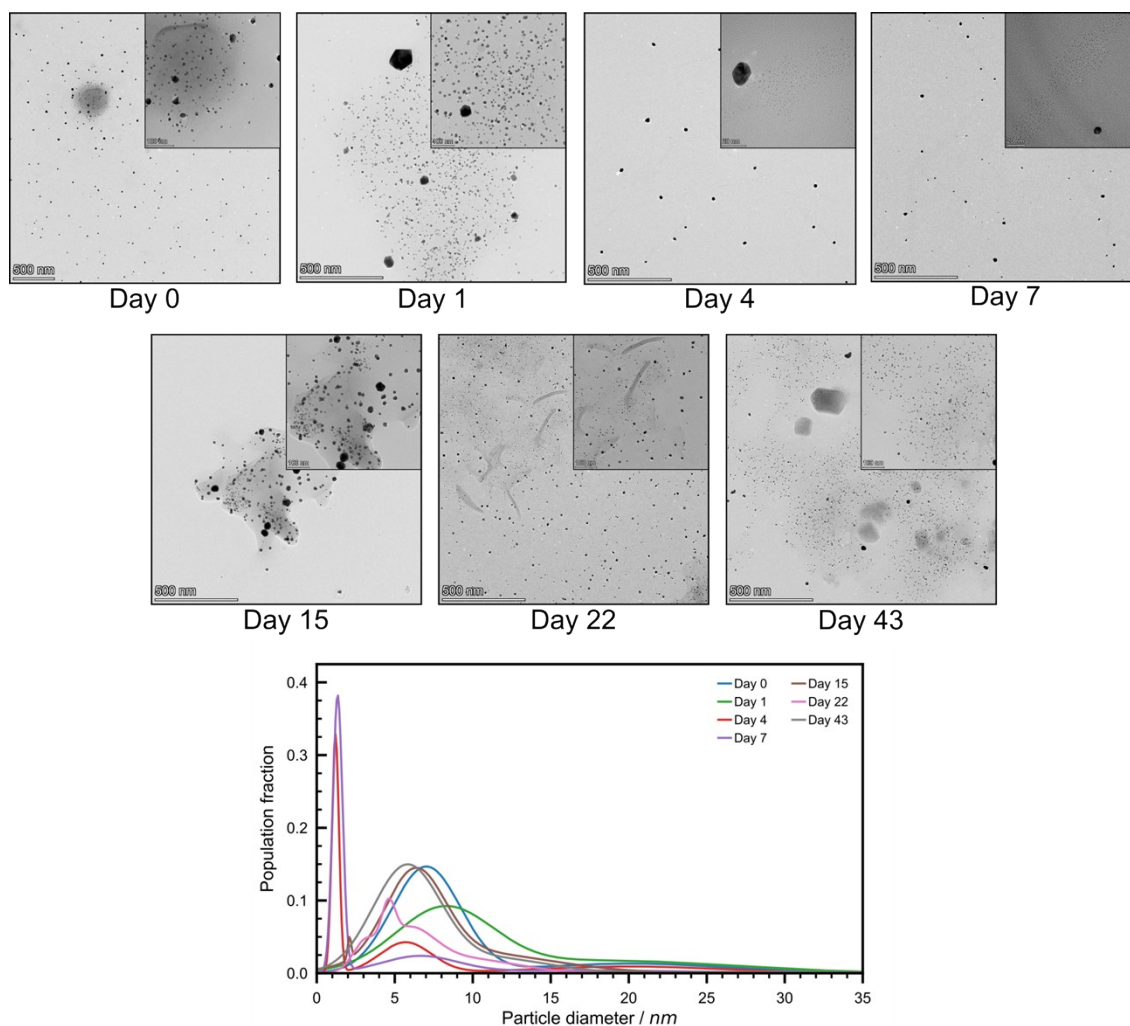
Figure S20 TEM results of room temperature aged milled powder. Representative TEM images and the population distribution profile of sized particles are shown for each day. Samples were analyzed after 0 (blue), 1 (green), 4 (red), 7 (violet), 15 (brown), 22 (pink), and 43 (grey) days of aging.

Table S1 Drop cast TEM peak table for nanoparticle distributions aged at 21 °C.

Peak[a]	Diameter (nm)						
	Day 0	Day 1	Day 4	Day 7	Day 15	Day 22	Day 43
1	7.0 ± 1.9	8.2 ± 2.6	1.2 ± 0.2	1.3 ± 0.3	2.1 ± 0.1	3.0 ± 0.6	5.8 ± 1.9
2	20.2 ± 5.1	18.3 ± 6.9	5.7 ± 1.4	6.6 ± 2.1	6.3 ± 1.6	4.6 ± 0.4	11.9 ± 2.6
3	-	-	20.0 ± 5.1	17.2 ± 5.8	9.7 ± 4.5	5.8 ± 1.4	-
4	-	-	-	-	-	9.6 ± 2.7	-

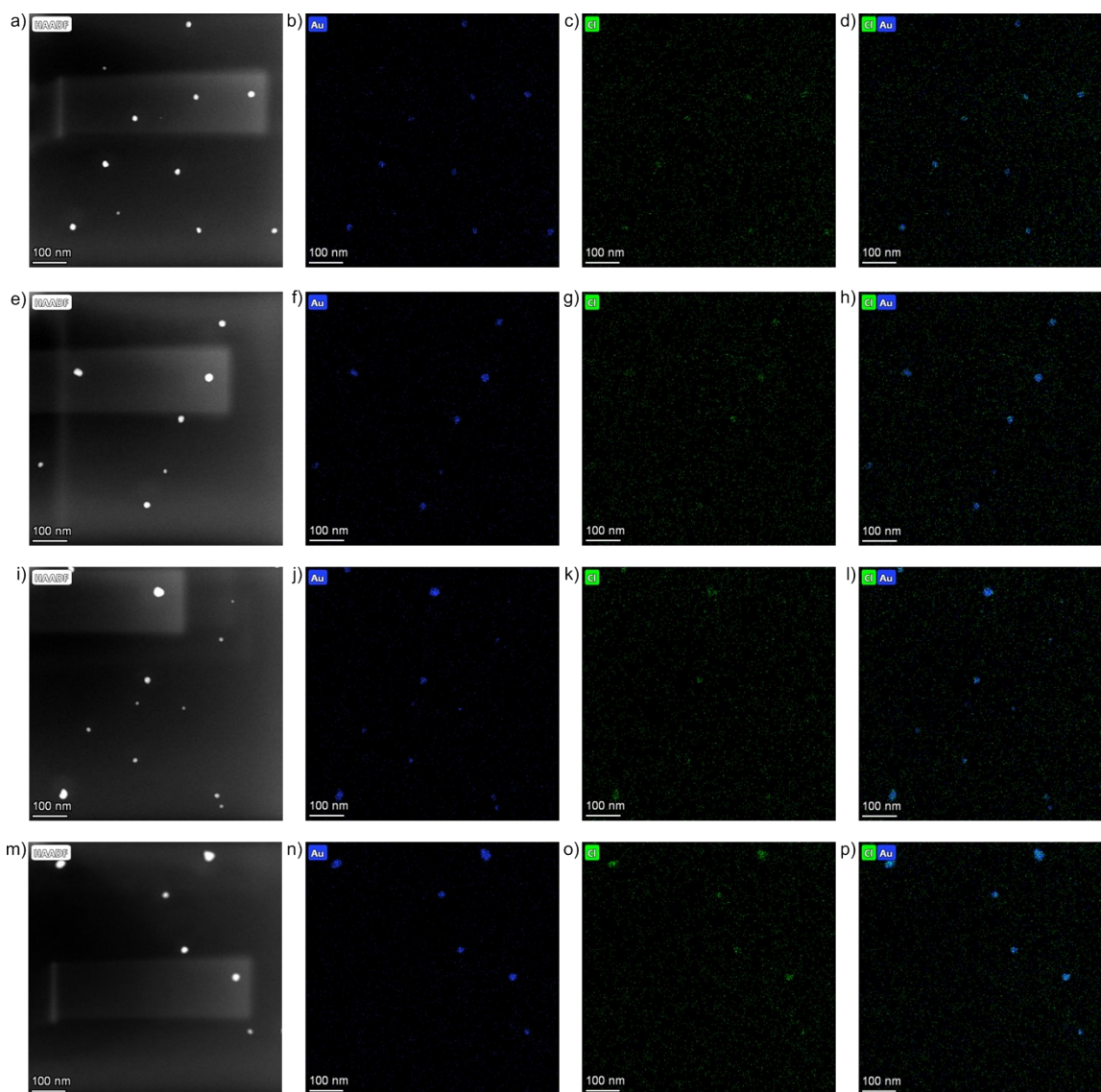[a] Ordered from smallest diameter to largest.

Figure S21 STEM-HAADF images and EDXS elemental maps for Au, Cl, and Au combined with Cl (left to right, respectively) for freshly milled powder (a-d), after one day of aging (e-h), after four days of aging (i-l), and after seven days of aging (m-p).
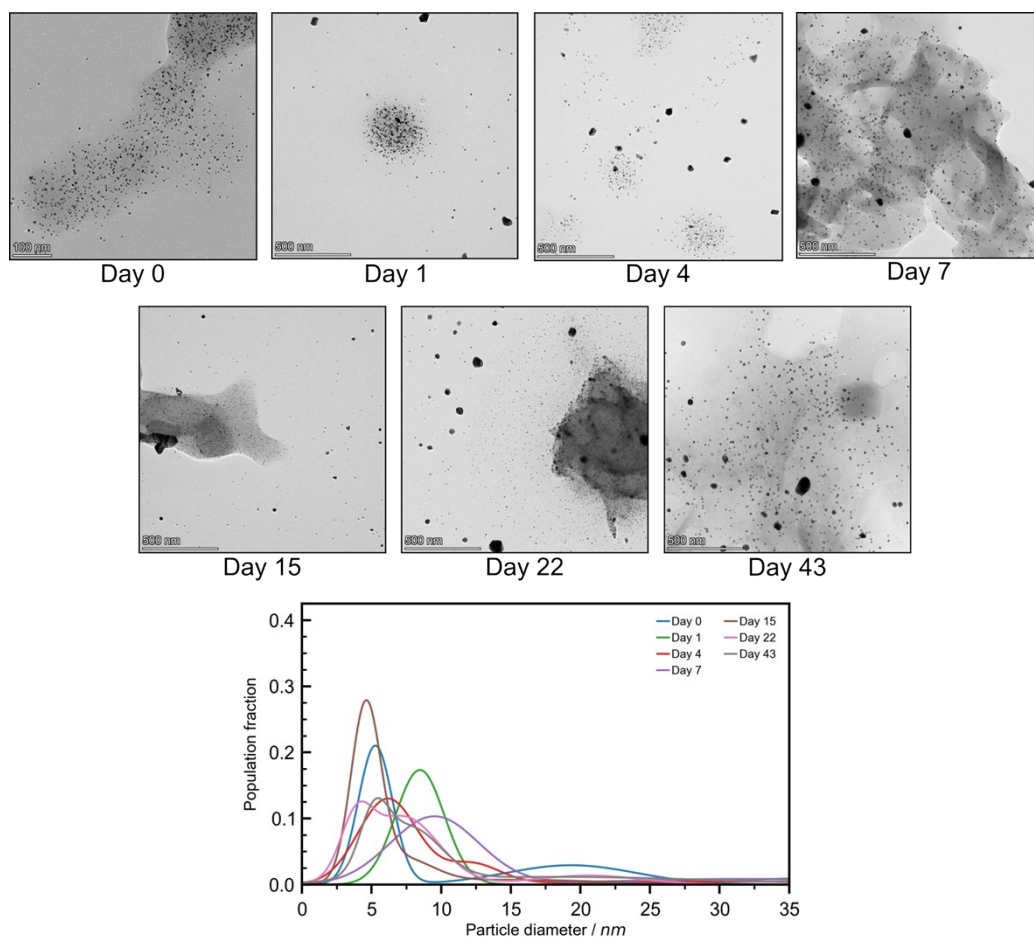
Figure S22 TEM results of low temperature aged milled powder. Representative TEM images and the population distribution profile of sized particles are shown for each day. Samples were analyzed after 0 (blue), 1 (green), 4 (red), 7 (violet), 15 (brown), 22 (pink), and 43 (grey) days of aging.

Table S2 Drop cast TEM peak table for nanoparticle distributions aged at -18 °C.

	Diameter (nm)						
Peak[a]	Day 0	Day 1	Day 4	Day 7	Day 15	Day 22	Day 43
1	5.3 ± 1.0	8.5 ± 1.5	6.2 ± 1.8	9.5 ± 2.7	4.6 ± 0.9	3.9 ± 1.0	5.2 ± 0.9
2	19.3 ± 3.9	37.8 ± 6.6	12.2 ± 1.7	31.4 ± 7.7	7.2 ± 1.8	7.3 ± 2.2	7.7 ± 1.9
3	-	-	32.7 ± 13.9	-	15.4 ± 5.1	20.6 ± 3.2	18.2 ± 9.4

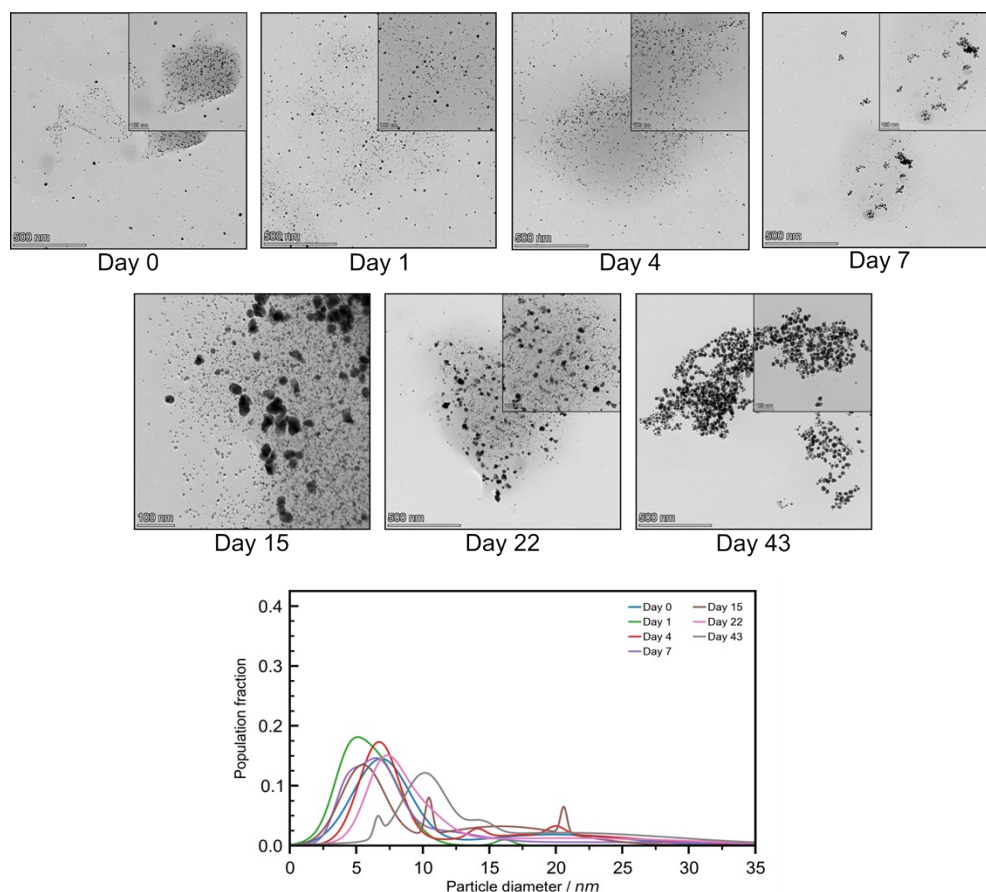[a] Ordered from smallest diameter to largest.

Figure S23 TEM results of elevated temperature aged milled powder. Representative TEM images and the population distribution profile of sized particles are shown for each day. Samples were analyzed after 0 (blue), 1 (green), 4 (red), 7 (violet), 15 (brown), 22 (pink), and 43 (grey) days of aging.

Table S3 Drop cast TEM peak table for nanoparticle distributions aged at 32 °C.

Diameter (nm)

Peak[a]	Day 0	Day 1	Day 4	Day 7	Day 15	Day 22	Day 43
1	6.9 ± 1.8	4.3 ± 0.9	6.7 ± 1.3	4.2 ± 0.8	5.5 ± 0.7	7.0 ± 1.1	6.6 ± 0.2
2	19.9 ± 4.4 4	6.2 ± 1.8	14.1 ± 0.5	6.5 ± 1.3	10.5 ± 0.2	9.1 ± 1.8	10.1 ± 1.4
3	-	16.1 ± 0.6	19.4 ± 5.8	10.6 ± 2.8	15.9 ± 4.2 4	20.5 ± 8.5	14.4 ± 0.8
4	-	-	20.0 ± 0.6	23.0 ± 9.8	20.6 ± 0.2	-	20.9 ± 7.5

[a] Ordered from smallest diameter to largest.

g. Activation energy of gold nanoparticle formation
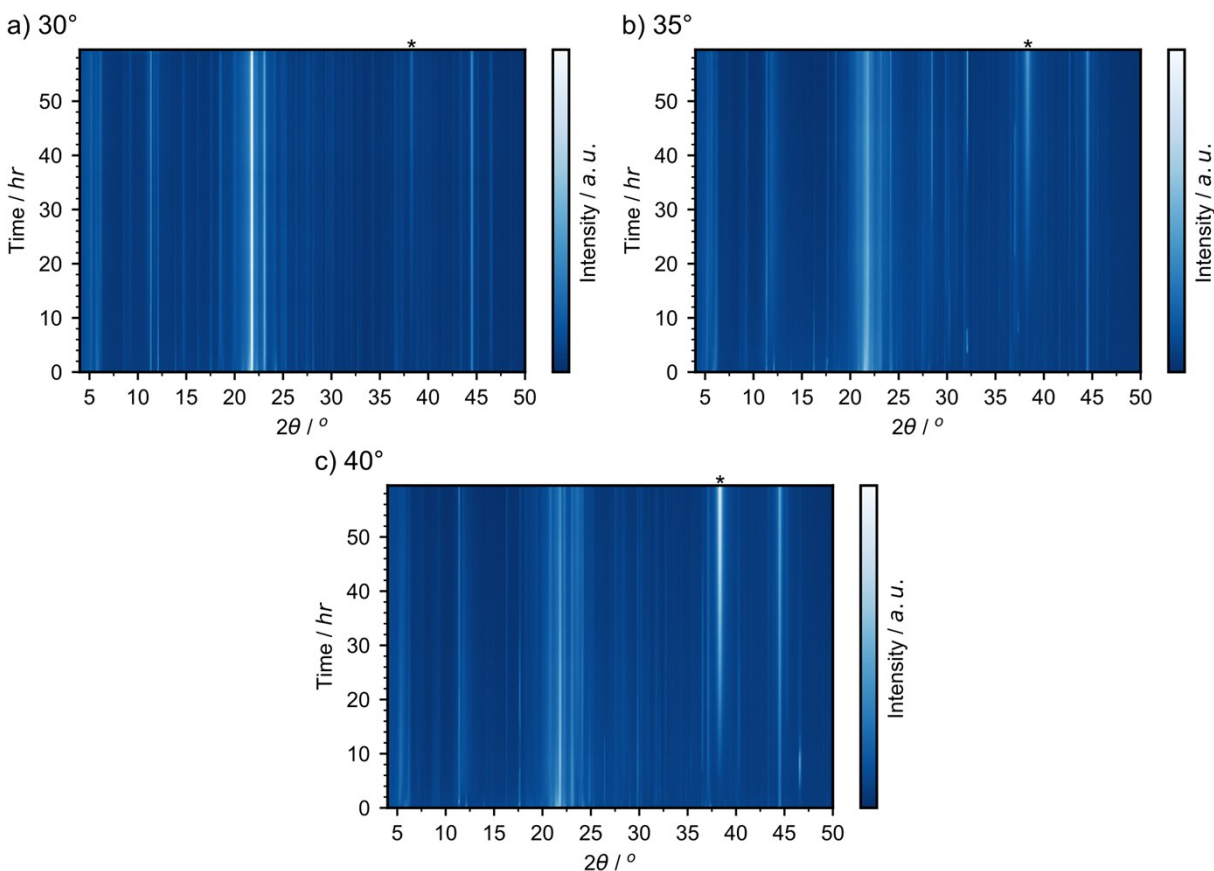
Constant temperature aging

Figure S24 *In situ* constant temperature powder X-ray diffraction analyses of AuNP formation at a) 30 °C, b) 35 °C, and c) 40 °C where * denotes the reflection corresponding to the (111) lattice place of elemental gold.

By integrating the diffractograms between 37.8° and 38.2° *2θ* the increase in intensity with respect to time was obtained, (Figure S25a), for each temperature. These were then fitted to a linear trendline, the gradient of which gives the rate of intensity increase for the gold temperature which is directly related to the formation of AuNPs. Plotting the natural logarithms of these rates against the inverse of the aging temperature allows for the activation energy to be obtained from the Arrhenius equation, Equation S3.

$$k = A \; exp^{-E_a/RT}$$ **Equation S3**

Where k is the rate, A is the pre-exponential factor, E_a the activation energy, R the molar gas constant, and T the temperature. Taking the natural log of both sides of the equation gives Equation S4.

$$ln(k) = ln(A) - E_a/RT$$ **Equation S4**

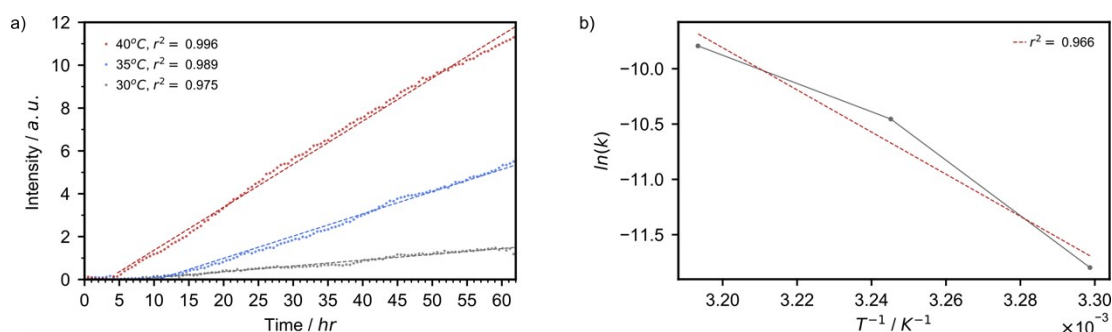Therefore, the gradient of the linear relationship in Figure S25b, is equal to $-E_a/R$.

Figure S25 a) Plot of the increase in intensity at 38.2° 2θ, i.e. the reflection corresponding to the (111) lattice plane of metallic gold, as a function of time when aged at 30 °C (grey), 35 °C (blue), and 40 °C (red) along with the corresponding linear fits. The linear fitting begins after five hours due to some sampling artefacts in the 35 °C experiment. b) Plot of the natural log of the rate of intensity increase, the gradient of the linear fits in panel (a), against the inverse of the aging temperature.

The activation energy for AuNP growth from the constant temperature PXRD studies was determined to be equal to 158.43 kJmol^{-1}.

Variable temperature aging

A similar analysis was performed for the variable temperature aging study (Figure S26a). Given the linear relationship between the intensity of the reflection at 38.2° 2θ observed in the constant temperature studies, linear fitting was performed for every five scans, leading to 12 individual rates. Each of which corresponding to one of the temperatures studied. Once again, the natural logarithms of these rates were plotted against the inverse of the temperature (Figure S26b).
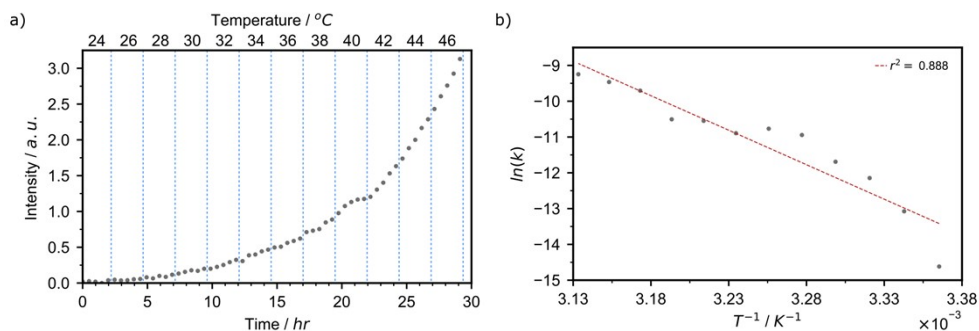
Figure S26 a) Plot of the increase in intensity at 38.2° 2θ, i.e. the reflection corresponding to the (111) lattice plane of metallic gold, as a function of time during variable temperature aging between 24 °C and 46 °C where the temperature is increased by 2 °C after every five consecutive measurements. b) Plot of the natural log of the rate of intensity increase against the inverse of the aging temperature.

Using the gradient of the linear trend in Figure S26b, the activation energy of AuNP growth was determine using Equation S4. In this case an activation energy of 160.33 kJmol⁻¹ was obtained.

The activation energies are in excellent agreement between the two studies.

$$\Delta E_a = E_a(VT) - E_a(CT) = 1.9 kJmol^{-1}$$

$$\langle E_a \rangle = 0.5[E_a(VT) + E_a(CT)] = 159.38 kJmol^{-1}$$

$$\%Err = 100\big(\delta/\langle E_a \rangle\big) = 1.20\%$$

h. Entropy of activation

Plots of the natural logarithms of these rates against the inverse of the aging temperature for the constant temperature (Figure S25b) and variable temperature (Figure S26b) PXRD aging studies can also be used to solve the Eyring equation (Equation S5) to obtain the entropy of activation.

$$k = \frac{\kappa k_B T}{h} exp^{\frac{\Delta S^{\ddagger}}{R}} exp^{-\frac{\Delta H^{\ddagger}}{RT}} \qquad \text{\textbf{Equation S5}}$$

Where k is the rate constant, T is the temperature, $\Delta H^{\ddagger}$ is the enthalpy of activation, R is the molar gas constant (8.3145 m² kg s⁻² K⁻¹ mol⁻¹),κ is the transmission coefficient, k_B is the

25

Boltzmann constant (1.3806 x10^{-23} m^2 kg s^{-2} K^{-1}), h is Planck's constant (6.6261 x10^{-34} m^2 kg s^{-1}), and $\Delta S^{\ddagger}$ is the entropy of activation. κ is assumed to be equal to one as it reflects the probability of the reaction proceeding after reaching the activated state. The Eyring equation can be solved through the line of best fit in Figure S25b and Figure S26b when rewritten as,

$$ln\left(\frac{k}{T}\right) = \frac{-\Delta H^{\ddagger}}{RT} \cdot \frac{1}{T} + ln\left(\frac{\kappa k_B}{h}\right) + \frac{\Delta S^{\ddagger}}{R} \qquad \textbf{Equation S6}$$

The *y* intercept (C) of the trend line is given by,

$$C = ln\left(\frac{\kappa k_B}{h}\right) + \frac{\Delta S^{\ddagger}}{R} \qquad \textbf{Equation S7}$$

$\Delta S^{\ddagger}$ can be obtained as,

$$\Delta S^{\ddagger} = R\left[C - ln\left(\frac{\kappa k_B}{h}\right)\right] \qquad \textbf{Equation S8}$$

$$\Delta S^{\ddagger} = 8.3145 \cdot (C - 23.7601) \qquad \textbf{Equation S9}$$

Therefore, the entropy of activation was calculated to be 227.73 J·mol^{-1} K^{-1} and 230.31 J·mol^{-1} K^{-1} for the constant temperature and variable temperature PXRD aging studies, respectively. Thus, the average entropy of activation for the mechanically-activated aging formation of AuNPs is 229.02 J·mol^{-1} K^{-1}. The positive entropy of activation confirms that the underlying process is dissociative in nature.